EDGE ARTICLE

Fluorinated trehalose analogues for cell surface engineering and imaging of *Mycobacterium tuberculosis*†

Collette S. Guy, [a] James A. Gott, [b] Jonathan Ramírez-Cárdenas, [c] Christopher de Wolf, [a] Christopher M. Furze, [a] Geoff West, [b] Juan C. Muñoz-García, [c] Jesus Angulo [c] and Elizabeth Fullam *[a]

The sensitive, rapid and accurate diagnosis of *Mycobacterium tuberculosis* (*Mtb*) infection is a central challenge in controlling the global tuberculosis (TB) pandemic. Yet the detection of mycobacteria is often made difficult by the low sensitivity of current diagnostic tools, with over 3.6 million TB cases missed each year. To overcome these limitations there is an urgent need for next-generation TB diagnostic technologies. Here we report the use of a discrete panel of native ^{19}F-trehalose (F-Tre) analogues to label and directly visualise *Mtb* by exploiting the uptake of fluorine-modified trehalose analogues *via* the mycobacterial trehalose LpqY-SugABC ATP-binding cassette (ABC) importer. We discovered the extent of modified F-Tre uptake correlates with LpqY substrate recognition and characterisation of the interacting sites by saturation transfer difference NMR coupled with molecular dynamics provides a unique glimpse into the molecular basis of fluorine-modified trehalose import in *Mtb*. Lipid profiling demonstrated that F-Tre analogues modified at positions 2, 3 and 6 are incorporated into mycobacterial cell-surface trehalose-containing glycolipids. This rapid one-step labelling approach facilitates the direct visualisation of F-Tre-labelled *Mtb* by Focused Ion Beam (FIB) Secondary Ion Mass Spectrometry (SIMS), enabling detection of the *Mtb* pathogen. Collectively, our findings highlight that F-Tre analogues have potential as tools to probe and unravel *Mtb* biology and can be exploited to detect and image TB.

Introduction

Mycobacterium tuberculosis (*Mtb*), the causative agent of tuberculosis (TB), continues to threaten humanity and remains a major health challenge, having claimed over 1.3 million lives in 2022.[1] Efforts to control the global TB pandemic have been jeopardised by the emergence of drug-resistant *Mtb* strains that are more complicated to treat and, in some instances, incurable.[1,2] Early diagnosis is crucial for the global management of TB since the timely intervention with antitubercular treatment regimens has the potential to prevent transmission, limit the emergence and spread of antibiotic resistant strains and save lives, yet each year over 3.6 million individuals do not receive treatment compounding the TB burden.[1,3,4] The current World Health Organisation approved TB diagnostics are limited to three main methods: microscopy, culture and nucleic acid amplification;[3,5] however, the low-cost microscopy-based tests used most widely in low-resource settings have limitations, which include low sensitivity.[6] Clearly, new molecular probes for improved, rapid, sensitive and accurate TB diagnostic technologies are needed.

As the architecture of the *Mtb* cell envelope is distinct from other species, comprising an interconnected peptidoglycan-arabinogalactan-mycolic acid (mAGP) core interspersed with a diverse array of mycobacterial specific 'free' lipids and glycolipids,[7–9] it provides a unique opportunity to develop *Mtb* pathogen specific reporter probes through utilisation of the specialised mycobacterial cell-wall assembly machinery for the direct incorporation of a detection moiety into the mycobacterial cell-envelope. Indeed, an array of fluorescent-based probes have been developed to monitor *Mtb* metabolism and image cell-envelope components, which have provided new insights into fundamental aspects of *Mtb* biology, including enzyme function, metabolism, cell wall biosynthesis and cell division.[10–15] Since the *Mtb* cell envelope is highly abundant in trehalose-containing glycolipids that include the mycolic acid esters: trehalose monomycolates (TMM) and trehalose

aSchool of Life Sciences, University of Warwick, Coventry, CV4 7AL, UK. E-mail: e.fullam@warwick.ac.uk; Tel: +44 (0)2476 574239

bWMG, University of Warwick, Coventry, CV4 7AL, UK

cInstituto de Investigaciones Químicas (IIQ), Consejo Superior de Investigaciones Científicas, Universidad de Sevilla, Avenida Américo Vespucio, 49, Sevilla, 41092, Spain

dimycolates (TDM), the acyltrehaloses comprising di- and polyacyltrehaloses and sulfoglycolipids, not typically found in other bacterial species,[7–9] recent attention has focused on the use of labelled trehalose derivatives for the visualisation of *Mtb*.[10–12,15–17] Incorporation of trehalose into mycobacterial cell-envelope glycolipids can proceed *via* two interlinked pathways: either through extracellular synthesis catalysed by the antigen 85 complex (Ag85)[18] and/or trehalose import[19] followed by biosynthesis of the TMM glycolipid within the cytoplasm (Fig. 1). The Ag85 complex, which include the secreted proteins Ag85A, Ag85B and Ag85C, is responsible for both the conjugation of extracellular mycolic acids to the arabinogalactan (AG) cell-wall core and the incorporation of a mycolic acid from one TMM into another TMM molecule to generate TDM.[18] Alternatively the 'free' trehalose moiety, released concomitantly during Ag85 mediated cell-wall biosynthesis, can be recycled *via* the LpqY-SugABC ATP-binding cassette transporter[19] and used as a precursor to yield cytoplasmic TMM, which is subsequently shuttled across the membrane by the MmpL3 exporter for insertion into the mycobacterial cell-envelope.[20,21] Recent studies identified that both pathways can be hijacked to incorporate modified trehalose analogues into mycobacterial cell-envelope trehalose mycolates. The Ag85 complex is known to be particularly promiscuous for a wide panel of extensively modified trehalose substrates[12] whereas the LpqY-SugABC importer only tolerates minor modifications.[11,16,22] Recent

structural and functional analysis of the LpqY substrate binding lipoprotein has afforded molecular level insights into the rules governing the precise substrate selectivity for this transporter enabling the design of reporter mimics to hijack this pathway.[22]

To date, trehalose probes possessing 'clickable' azide and alkyne reactive handles have been used extensively for imaging of mycobacteria,[11,12,16,23,24] however this approach requires extensive wash steps and a secondary, bulky fluorophore label for the direct visualisation of the cells, limiting their use. An ^{18}F trehalose-modified radioprobe can be used to label the non-pathogenic model *Mycobacterium smegmatis* organism.[17,25] However, this direct approach is challenging as fluorine-18 has a short half-life ($\sim$109 minutes) and it is not possible to infer labelling of pathogenic *Mtb* because of the significant differences in nutrient uptake and processing between these diverse mycobacterial species.[26–28] To address these potential limitations we rationalised we could leverage the *Mtb* LpqY-SugABC transporter to develop and deliver native ^{19}F-modified trehalose reporter probes as a direct route to specifically visualise mycobacteria by focused ion beam (FIB) secondary ion mass spectrometry (SIMS), a technique which is increasingly being applied as a powerful tool to map elemental ions and molecules in biological samples.[29–31] SIMs is an analytical technique that uses a focused ion beam to scan the sample surface, generating secondary ions detected by a mass analyser.[32] Analysis of the mass spectrum generated on a pixel-by-pixel basis produces an
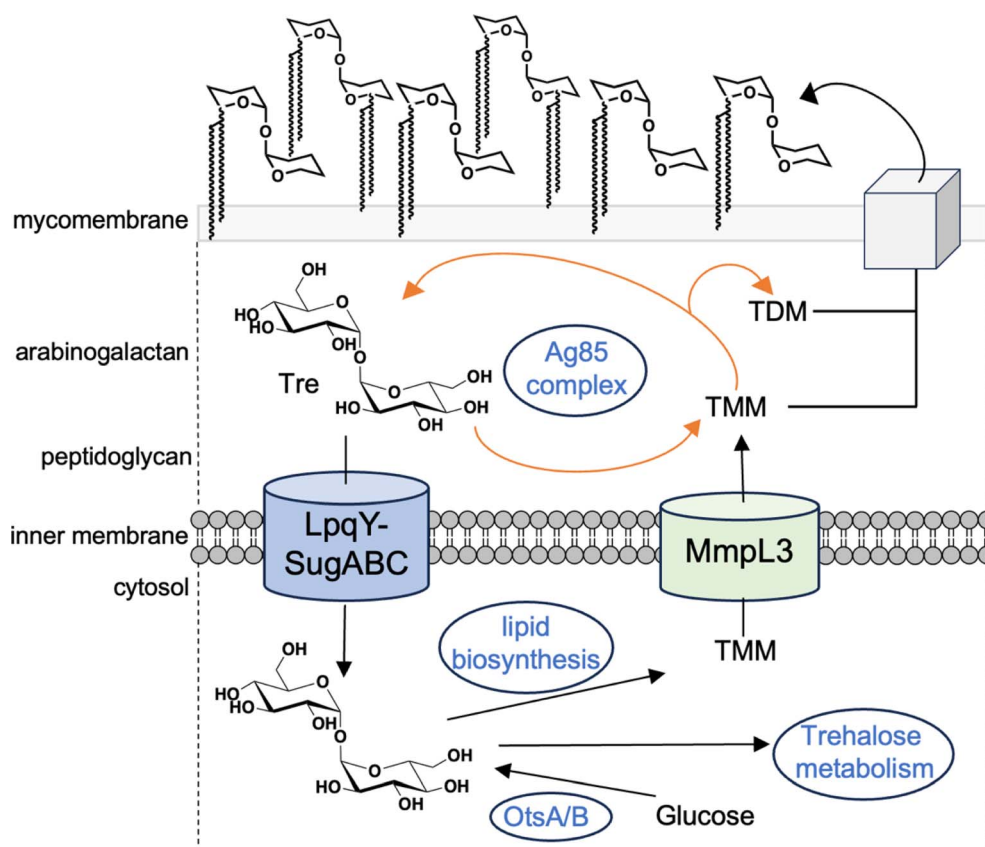

Fig. 1 Schematic illustrating the pathways involved in trehalose processing in mycobacteria. TMM: trehalose monomycolate; TDM: trehalose dimycolate.

'ion image' of the composition, distribution and intensity of elements/molecules with spatial resolution within a sample.

We show here that a discrete panel of unnatural fluorine modified trehalose analogues are indeed tolerated by the *Mtb* LpqY-SugABC transporter and reveal the molecular architecture dictating their specific recognition. Subsequent characterisation demonstrated that this transport promiscuity can be harnessed to facilitate the uptake of fluorinated trehalose probes into live *Mtb* cells, which are subsequently incorporated into extracellular mycobacterial trehalose containing mycolic acids, enabling detection of the *Mtb* pathogen. Taken together, these results highlight the possibility of exploiting native fluorinated-trehalose derivatives to be used not only as tools for unravelling *Mtb* biology but also as new molecular probes for the direct visualisation and detection of *Mtb*.

Results and discussion

Panel of fluorinated trehalose analogues

To explore the potential of fluorinated trehalose for *Mtb* detection and evaluate how selected modifications influence assimilation and cell-labelling, we synthesised a panel of fluorinated trehalose analogues with systematic modifications at either the 2-, 3-, 4-, or 6-position on one glucose subunit with retention of the natural stereochemistry (**2–5**). An established chemoenzymatic route[33] was employed to access 2-deoxy-2-fluorotrehalose (2F-Tre) (**2**), 3-deoxy-3-fluoro-trehalose (3F-Tre) (**3**) and 6-deoxy-6-fluoro-trehalose (6F-Tre) (**5**) in 42–49% yield, and a modified five-step synthetic route[17,34] (Scheme S1†) afforded 4-deoxy-4-fluoro-trehalose (4F-Tre) (**4**), giving the focused panel shown in Fig. 2 (details provided in ESI, Schemes S1, Fig. S12–S30 and characterisation data†).

LpqY substrate specificity for F-Tre analogues

As the mycobacterial specific LpqY-SugABC transporter is solely responsible for the import of trehalose,[11,19,22] our first goal was to establish if the introduction, and position, of a fluorine moiety impacts on substrate recognition. We assessed the binding affinity of each fluorinated analogue (**2–5**) to LpqY, the substrate-binding domain that dictates substrate specificity and hence, subsequent transport, by microscale thermophoresis

(MST). Highest binding affinities (K_d) were observed for 3F-Tre (110.8 ± 7.1 μM) and 6F-Tre (90.3 ± 0.9 μM) with comparable affinities to unmodified trehalose (109.5 ± 3.2 μM) whereas 2F-Tre and 4F-Tre bind ∼8- and ∼16-fold more weakly, with 4F-Tre having affinity in the millimolar range (Table 1, Fig. S1†). Altogether, these findings indicate that the position of the fluorine modification is key to LpqY recognition with replacement at the 3- or 6-positions preferred. This is in direct contrast to previous LpqY-azide-trehalose binding analyses (Table 1)[22] that identified preferential binding of azide-trehalose modified at the 4- > 6- ≥ 3- > 2-positions, albeit with ∼2–4 weaker affinity than the corresponding fluorinated versions, highlighting the importance of both the substituent type and position in transporter-substrate tolerance and recognition.

Molecular basis of F-Tre analogue recognition

Having established that LpqY has the capacity to recognise fluorinated trehalose analogues we sought to determine the molecular rules of recognition in solution. Saturation transfer difference (STD) NMR confirmed binding for each fluorinated trehalose analogue, verifying that switching a hydroxyl group to fluorine at all possible positions is not detrimental for recognition by the mycobacterial trehalose transporter (Fig. 3). The STD NMR intensities differed depending on the temperature of the experiment (Fig. S2–S3 and Tables S1–S4†). More intense signal intensities were observed at low temperature (5 °C) for

Table 1 Binding affinity analysis of LpqY to F-Tre analogues[a]

Substrate	K_d (μM)	Reference
Trehalose	109.5 ± 3.2	This study
2-Deoxy-2-fluoro-trehalose (2F-Tre)	770.4 ± 23.2	This study
2-Deoxy-2-azido-trehalose (2Az-Tre)	1915.6 ± 7.7	22
3-Deoxy-3-fluoro-trehalose (3F-Tre)	110.8 ± 7.1	This study
3-Deoxy-3-azido-trehalose (3Az-Tre)	474.9 ± 17.2	22
4-Deoxy-4-fluoro-trehalose (4F-Tre)	1483.7 ± 75.6	This study
4-Deoxy-4-azido-trehalose (4Az-Tre)	246.6 ± 7.1	22
6-Deoxy-6-fluoro-trehalose (6F-Tre)	90.3 ± 0.9	This study
6-Deoxy-6-azido-trehalose (6Az-Tre)	442.7 ± 5.3	22

[a] Mean ± standard error mean is from at least three independent experiments. The substrate structures are shown in Fig. 2. The binding affinity data is shown in Fig. S1.
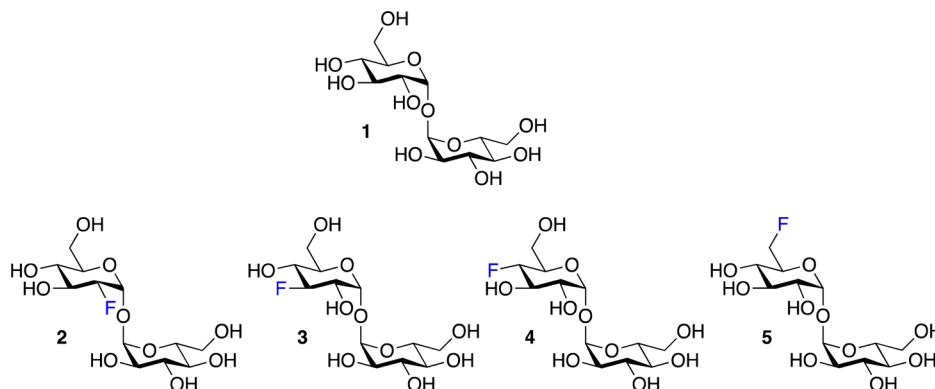

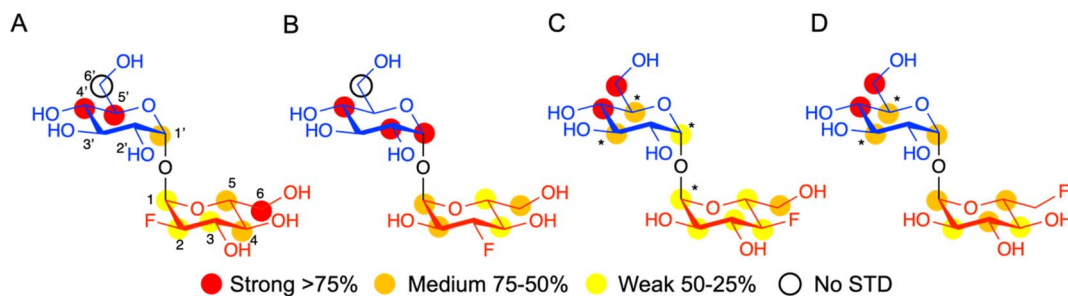**Fig. 2** Panel of fluorinated trehalose analogues.

Fig. 3 STD NMR binding epitope mapping of F–Tre analogues (2–5) to LpqY. Binding epitope map of (A) 2F-Tre, (B) 3F-Tre, (C) 4F-Tre and (D) 6F-Tre. Protein saturation was achieved by irradiation at 0.53 ppm for (A) and (C), whereas irradiation was at 0.84 ppm for (B) and (D). The coloured spheres represent normalized STD NMR intensities. STD responses are only indicated for protons that could accurately be measured. Asterisks indicate averaged STD values due to overlapping. Glc-1 (blue), Glc-2 (red), STD NMR, saturation transfer difference NMR.

2F-Tre and 4F-Tre, whereas a higher temperature of 30 °C was required for STD NMR observation of 3F-Tre and 6F-Tre, especially in the case of the 3-fluoro derivative where the particularly low signal-to-noise ratio meant no STD NMR analysis was possible at 5 °C. These results indicate a much stronger affinity for 3F-Tre and 6F-Tre, in comparison with the 2- and 4-fluoro derivatives, consistent with our binding affinity data (Table 1). STD binding epitope maps are unique for each F-Tre analogue (Fig. 3) and indicate that protons from both the unmodified and

modified carbohydrate rings make distinct close contacts to LpqY relevant for recognition, with a significant overall decrease in the relative STD intensities at the modified fluorinated glucose ring (Fig. 3).

Comparative DEEP-STD NMR analyses,[35] which assess the type of protein residue that makes contacts with the fluorinated trehalose analogues (Fig. S4†), in combination with molecular dynamics simulations over 100 ns (Fig. S5†) revealed the relative orientations of the four ligands in the LpqY binding pocket
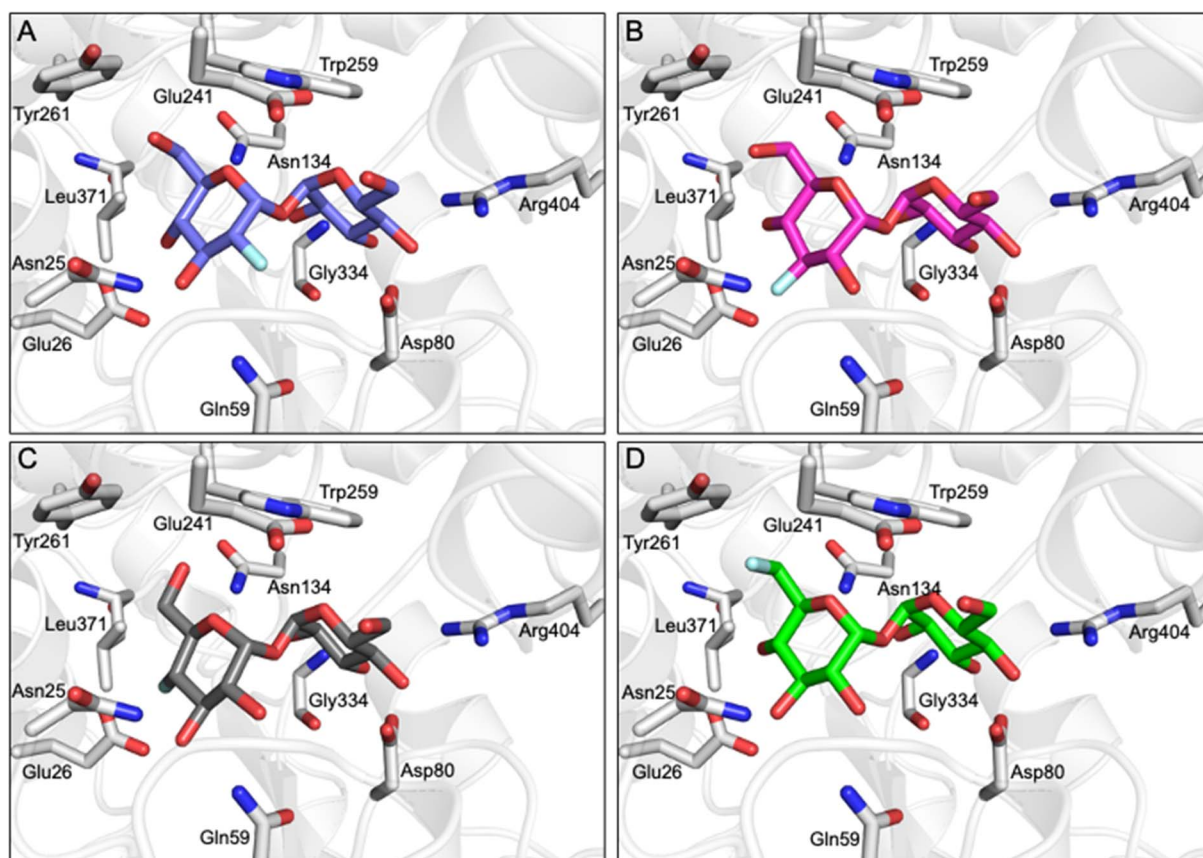

Fig. 4 F–Tre binding to LpqY. Model of the mode of binding of F–Tre analogues based on experimentally derived DEEP-STD NMR derived interactions and molecular dynamic simulations. (A) 2F-Tre (blue carbon atoms), (B) 3F-Tre (magenta carbon atoms), (C) 4F-Tre (dark grey carbon atoms), and (D) 6F-Tre (green carbon atoms). Cartoon representation of LpqY in grey (PDB 7APE), trehalose and binding site residues are represented as sticks (oxygen: red; fluorine: pale blue).

Chemical Science

View Article Online

Edge Article

Open Access Article. Published on 12 August 2024. Downloaded on 2/8/2026 10:59:39 PM. This article is licensed under a Creative Commons Attribution 3.0 Unported Licence.

(Fig. 4). Each of the F-Tre analogues bind in similar relative orientations and sit in an analogous position to trehalose (PDB 7APE)[22] (Fig. S6†). The fluorinated-modified glucose ring is located towards the entrance of the substrate binding cavity, similar to the orientation we observed previously for 6Az-Tre,[22] indicating that when the second glucose ring is modified it is preferentially accommodated within an expanded binding pocket at the channel entrance rather than buried at the base of the binding cleft (Fig. 4). Because the sidechains of Asn25, Glu26, Gln59 and Asn134 make hydrogen bond contacts with the modified glucose ring it is clear this interaction network plays an important role in controlling fluoro-modified trehalose specificity. Indeed, the significantly reduced affinity of 4F-Tre could be attributed to weakened interactions through the loss of a hydrogen-bond partner with Glu26 when a fluorine group is substituted at the 4-position.

Mtb imports 2F-, 3F- and 6F-Tre analogues *via* the LpqY-SugABC transporter

Having confirmed that the fluorinated trehalose analogues bind to LpqY, and since not all substrates recognised by periplasmic
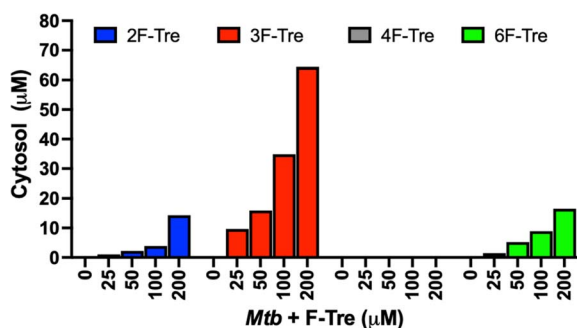

Fig. 5 Ion chromatography analysis of F-Tre labelled *Mycobacterium tuberculosis*. *Mtb* was cultured in the presence of F-Tre analogues **2–5** (0–200 μM) and the cytosolic extracts analysed by high performance anion exchange chromatography with pulsed amperometric detection (HPAEC-PAD), and F-Tre concentration quantified. The ion-chromatography traces and retention times are shown in Fig. S7 and Table S5.†

binding domains are translocated by the cognate ABC transporter, we sought to evaluate whether these derivatives are taken up by live *Mtb* cells by ion chromatography. Treatment of *Mtb* cells with each fluorinated analogue led to a significant dose-dependent increase in the accumulation of 2F-Tre, 3F-Tre and 6F-Tre in *Mtb* cells, with the assimilation of micromolar levels even after exposure to the lowest concentration of the probe (25 μM) (Fig. 5). No uptake of 4F-Tre was detected, a finding consistent with its poor binding affinity to LpqY. The uptake pattern matches the entry of these analogues into non-pathogenic *M. smegmatis* cells, suggesting overlapping fluorine-modified trehalose analogue recognition profiles between these bacilli.[17] These findings, together with the determined F-Tre analogue affinities for LpqY, emphasise the importance of the LpqY substrate binding domain in controlling which substrates are translocated.

As *Mtb* efficiently imports the 2-, 3- and 6-fluorinated trehalose derivatives we then asked how rapidly each analogue is accumulated. We evaluated uptake in cytosolic extracts and calculated accumulation rates of 0.80 μM h^{-1} (2F-Tre) 0.94 μM h^{-1} (3F-Tre) and 0.82 μM h^{-1} (6F-Tre). Rapid uptake of each F-Tre derivative was observed at 30 min and at 8 hours ~20% increased accumulation of 3F-Tre was detected compared to 2F- and 6F-Tre (Fig. 6, S8 and Table S6†). In agreement with previous studies that used radiolabelled ^{14}C-trehalose,[19] no saturation of uptake was observed for each F-Tre analogue **2**, **3** and **5**, indicating that an equilibrium between trehalose import and export has not yet been reached at the 8 hour timepoint, which may be consistent with the extremely slow growth rate of the *Mtb* bacillus or metabolic utilisation of the imported F-Tre analogues. Altogether, these observations establish that 2F-, 3F- and 6F-trehalose are rapidly transported, and accumulate, in live *Mtb* cells.

We then asked whether the F-Tre analogues are imported *via* LpqY-SugABC transporter or *via* an alternative route and evaluated uptake in a *Mycobacterium bovis* BCG strain lacking the trehalose transporter (*ΔlpqY-sugABC*),[11] as a model for *Mtb*. In agreement with our *Mtb* data 2F-, 3F- and 6F-Tre accumulate in wild-type *M. bovis* BCG cytosolic extracts and not 4F-Tre (Fig. 7). Notably, uptake of each F-Tre derivative was completely abolished in the *ΔlpqY-sugABC* mutant and transport restored in the
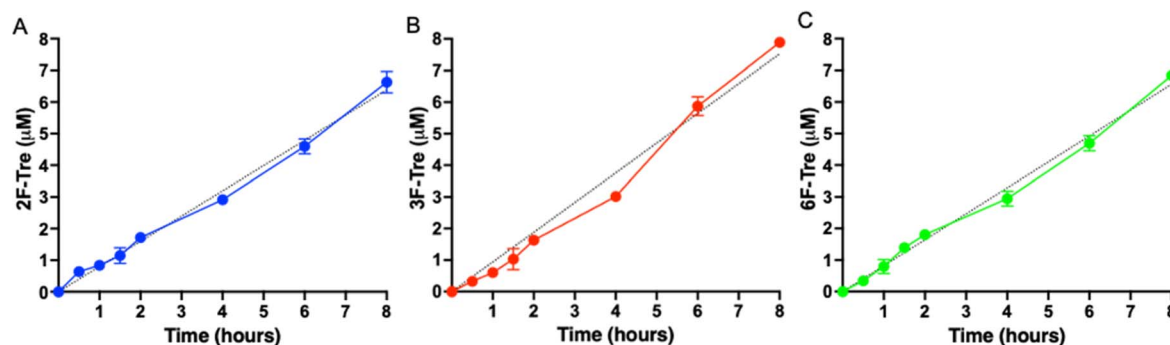

Fig. 6 Time dependent uptake of F-Tre analogues in *Mycobacterium tuberculosis*. *Mtb* was cultured in the presence of (A) 2F-Tre, (B) 3F-Tre and (C) 6F-Tre (100 μM) and the cytosolic extracts sampled at the time points indicated and analysed by high performance anion exchange chromatography with pulsed amperometric detection (HPAEC-PAD). Error bars denote the standard deviation from duplicate experiments. Simple linear regression fit is shown with a black dotted line (A) $y = 80x$; (B) $y = 0.94x$; (C) $y = 0.82x$. The concentration values are in Table S6.† Representative ion-chromatography traces are shown in Fig. S8† and retention times are in Table S7.†
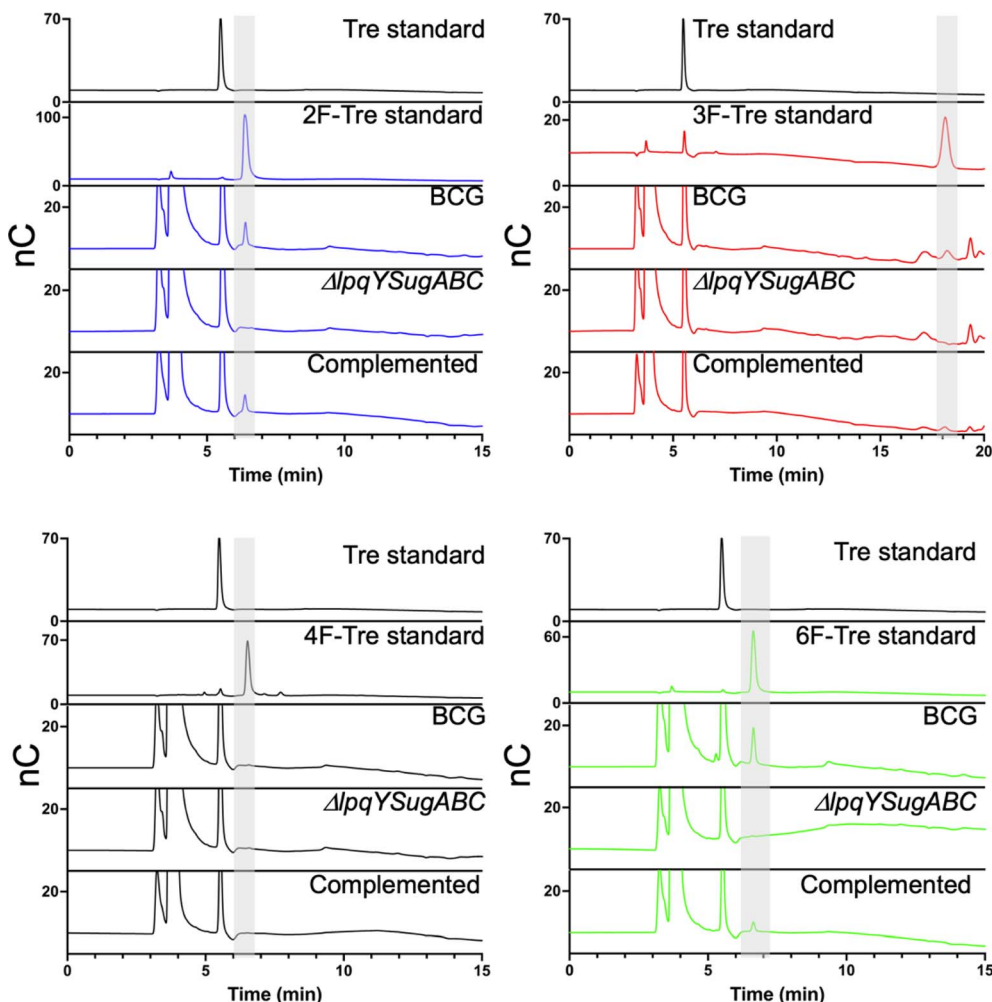
13970 | *Chem. Sci.*, 2024, **15**, 13966–13975

© 2024 The Author(s). Published by the Royal Society of Chemistry

Fig. 7 Comparison of F-Tre uptake in *Mycobacterium bovis* BCG and LpqY-SugABC mutant strains. Wild-type *Mycobacterium bovis* BCG and the *ΔlpqY-sugABC Mycobacterium bovis* BCG mutant and complemented strain *Mycobacterium bovis* BCG *ΔlpqY-sugABC::lpqY-SugABC* were cultured in the presence of F-Tre analogues **2**, **3**, **4** and **5** (100 μM) and the cytosolic extracts analysed by high performance anion exchange chromatography with pulsed amperometric detection (HPAEC-PAD). Retention times and peak areas are in Table S8.†

corresponding complemented strain. Taken together, as the mutant strain is unable to utilise F-Tre, these data clearly show that uptake of fluorinated trehalose analogues occurs solely *via* the trehalose LpqY-SugABC import system.

Mtb incorporates 2F-, 3F- and 6F-Tre analogues into trehalose-containing glycolipids

To determine the fate of F-Tre analogues following import across the mycobacterial cell-envelope *Mtb* and *M. bovis* BCG were exposed to each F-Tre analogue (**2–5**, 100 μM), alongside trehalose and untreated cells, and the extracted lipids evaluated by thin layer chromatography (TLC) and ion chromatography (Fig. 8, S9 and Table S9†). Treatment of *Mtb* and *M. bovis* BCG with 2F-, 3F- and 6F-Tre afforded new spots in the lipid extracts that were not present in the control samples (Fig. 8). No new spots were observed with 4F-Tre addition, consistent with its lack of uptake. Two additional lower polarity bands than TMM are present for the 2F- and 3F- samples and one for 6F-Tre (Fig. 8), indicating their incorporation into TMM (Fig. 8). This

labelling pattern is consistent with two possible fluorinated-TMM regiochemistries for 2F- and 3F-Tre, where the fluorine is either on the same glucose moiety as the mycolic acid or the other subunit (Fig. 8). Since the TMM 6-position is blocked through mycolic attachment, only one 6 F trehalose isomer is possible, as observed (Fig. 8). The presence of one additional lower polarity TDM band for 2F- and 3F-Tre suggests these analogues are also incorporated into the TDMs. As expected, when mycobacteria are labelled with 6F-Tre no additional band in the TDM region is observed, since both 6-positions are inaccessible due to the attachment of mycolic acids on both glucose rings preventing the production of 6-fluorinated TDM.

Altogether, these experiments demonstrate that, unless the 4-position is modified, mycobacteria have the capacity to take up fluorinated trehalose analogues and incorporate these modified sugars into cell-surface trehalose mycolates. It is notable that 4F-Tre is not found in any trehalose glycolipid in either *Mtb* or *M. bovis* BCG as this differs from the situation found for the analogous azido-trehalose derivatives which are
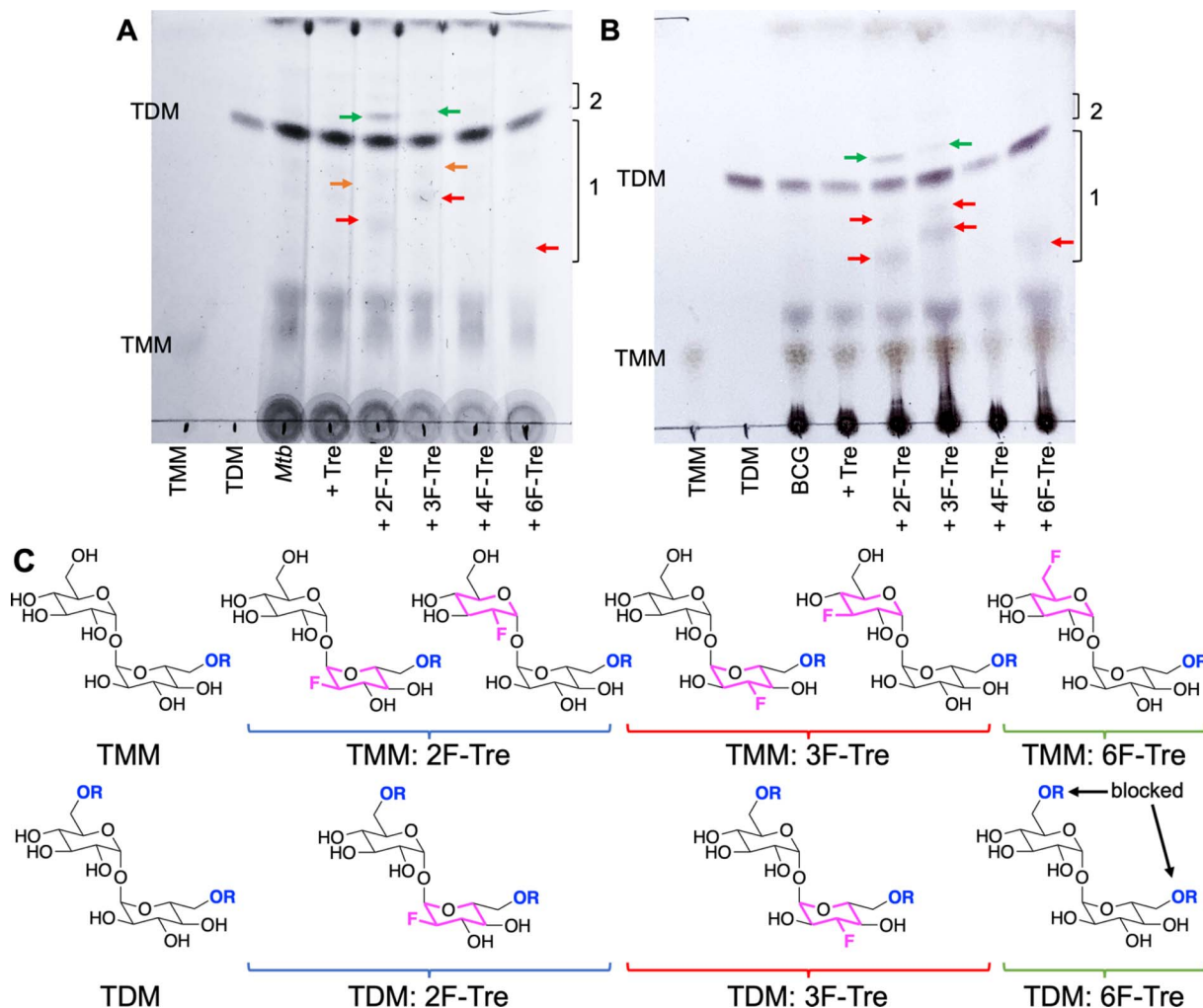
Fig. 8 Thin layer chromatography analysis of *Mtb* and *M. bovis* BCG lipids after labelling with F‑Tre analogues. (A) *Mtb* extracted apolar lipids. (B) *M. bovis* BCG extracted apolar lipids. (C) Structures illustrating potential F‑Tre TMM and TDM modifications. Red arrows indicate new spots with intermediate polarity compared to TMM and TDM standards in region 1; green arrows indicated new spots which are less polar than TDM in region 2; orange arrows indicate new spots with intermediate polarity compared to TMM and TDM standards in region 1 that are visible directly on the TLC plate but not as clearly visible on the image. The image has been contrast adjusted to improve the visualization of spots. TMM: trehalose monomycolate standard, TDM: trehalose dimycolate standard.

all incorporated into mycobacterial glycolipids, albeit *via* different routes, depending on the mycobacterial species.[11,17] For example, in *M. bovis* BCG, 3‑ and 4‑azido trehalose are not recycled *via* LpqY-SugABC but, instead, incorporated into TMM and TDM by the extracellular Ag85 complex.[11] Yet this does not occur for any F‑Tre analogue. Thus, these findings reveal distinct mechanistic pathways for trehalose analogue recognition and use, which depend on both the type and position of modification and the mycobacterial species, highlighting an evolutionary divergence of trehalose transport across mycobacterial species.

Mtb does not readily metabolise 2F-, 3F- and 6F-Tre analogues into corresponding glucose analogues

Next, to determine if the fluorinated-trehalose derivatives are processed further we analysed the same cytosolic extracts of *Mtb* exposed to **2**, **3**, and **5** (100 μM) for the presence of fluorinated-

glucose break-down products that would result from trehalase activity: 2-deoxy-2-fluoro-glucose (2F-Glc), 3-deoxy-3-fluoro-glucose (3F-Glc) and 6-deoxy-6-fluoro-glucose (6F-Glc) respectively (Fig. S10 and Table S10†). No cytosolic 3F- or 6F-glucose were found, indicating that the cleavage of 3F- and 6F-Tre does not occur. This suggests that intact 3F- and 6F-Tre are predominantly processed by pathways that ultimately incorporate these derivatives into cell-surface trehalose glycolipids. In contrast, *Mtb* labelled with 2F-Tre revealed the presence of low levels of 2F-Glc, indicating some degradation occurs, likely catalysed by the *Mtb* trehalase.[36] It is possible that the 2F-Glc metabolite is then diverted into alternative glucose utilisation pathways and not solely incorporated into cell-surface trehalose opening up potential off-target labelling routes. As the F-Tre analogues effectively label *Mtb* glycolipids, we did not explore additional metabolic pathways. However the F-Tre analogues might also be metabolised by intracellular enzymes such as
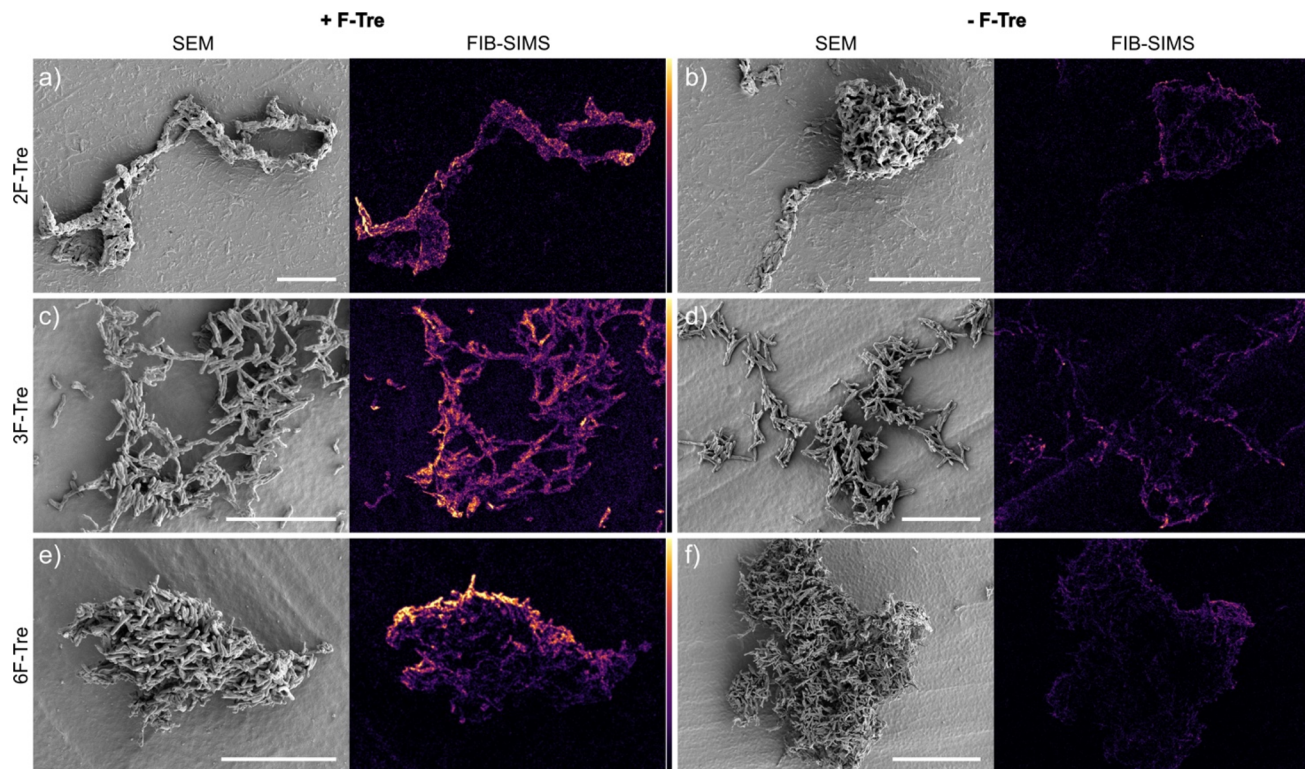
Fig. 9 F-Tre labelled *Mtb* scanning electron microscope (SEM) images and focused ion beam–secondary ion mass spectrometry (FIB-SIMS) maps of *Mtb* cells treated with (a) 2F-Tre, (c) 3F-Tre (e) 6F-Tre (100 μM) and untreated control cells (b), (d) and (f). Colour scale represents $^{19}F^-$ SIMS counts, black = lowest intensity, yellow = highest intensity. White scale bar 10 μm (a, c, d and e), 20 μm (b and d).

TreS, which isomerises trehalose to maltose, or through phosphorylation.

Imaging F-Tre labelled *Mtb* by secondary ion mass spectrometry

As fluorine-modified trehalose analogues are incorporated into cell-surface trehalose-containing *Mtb* glycolipids, we next examined the ability to visualise and image F-Tre labelled *Mtb* cells using focused ion beam (FIB) secondary ion mass spectrometry (SIMS), focused on $^{19}F^-$ ions. Elemental scanning for negative ions in the mass range 1–100 detected $^{19}F^-$ fluorine ions in all *Mtb* samples exposed to F-Tre and only trace levels in non-treated cells (Fig. S11† and 9). We then mapped the distribution of fluorine in the samples, first imaging the *Mtb* cells by scanning electron microscopy (SEM) to show the morphology of the cells and then analysis of the same section by FIB-SIMS. The intensity of the SIMS $^{19}F^-$ signal correlated with the scanning electron micrograph and showed a clear pattern of accumulation and localisation of F-Tre in treated *Mtb* cells (Fig. 9). In contrast only background $^{19}F^-$ levels were observed in untreated cells. Crucially, our findings establish that F-Tre labelling of live *Mtb* cells affords a prominent $^{19}F^-$ SIMS signal and low background demonstrating the feasibility of this approach for the direct detection and imaging of mycobacteria. Whilst robust labelling is observed for each probe, it is conceivable that the incorporation of multiple fluorine atoms on the same glucose ring that combines modifications at either the 2- 3-, or 6-positions could enhance the signal intensity further.

Conclusions

One of the major hurdles in controlling the TB pandemic is the need for improved TB diagnosis. One route to achieve this is to transition from sputum microscopy to molecular testing. Yet molecular probes for the direct detection of TB are lacking. To address this deficiency, we used native fluorinated trehalose probes for imaging by FIB-SIMS, providing unique opportunities to specifically visualise and detect the *Mtb* pathogen. Given the requirement for specialised mass-spectrometry imaging equipment, optimisation will be necessary for use in resource limited settings. However 19-fluorine labelled probes may offer advantages over 18-fluorine methods, which have short half-lives, especially where point-of-care analysis is unfeasible and instead requires sample collection and central testing facilities. In conclusion, here we have clearly shown that we can hijack the promiscuity of the mycobacterial specific LpqY-SugABC trehalose transport machinery to incorporate fluorinated reporters into mycobacterial specific cell-surface glycolipids, combined with FIB-SIMS imaging to resolve $^{19}F^-$ localisation and directly image *Mtb* cells. Moreover, our findings demonstrate that F-Tre probes allow for the detection of the *Mtb* pathogen with high sensitivity. Expanding on this, our studies reveal a discernible dependence on the position of fluorine atom modification for efficient *Mtb* labelling. Specifically, we have uncovered the molecular framework that dictates probe recognition and import allowing us to explain F-Tre selectivity. We have shown that a single fluorine modification at the 2-, 3- and 6-positions of

one glucose ring is optimal since substitution at the 4-position disrupts a critical hydrogen bond interaction that significantly weakens interactions with LpqY, impeding 4F-Tre import. The structural insights into F-Tre recognition and uptake analysis provided by this study, combined with FIB-SIMS imaging of *Mtb* cells provides a firm foundation that open opportunities for the rational development of high-contrast molecular probes for the detection of mycobacteria and provides an important step towards expanding the existing toolbox of molecular reporters for TB diagnosis.

Data availability

The data supporting this article have been included as part of the ESI.†

Author contributions

Conceptulisation: CSG, EF; methodology: CSG, JAG, JRC, JCMG, CdW, EF; formal analysis: CSG, JAG, JRC, JCMG, JA, EF; investigation: CSG, JAG, JRC, GW, JCMG, CMF, EF; resources: JA; visualisation: CSG, JAG, JRC, JCMG, EF; supervision: GW, JCMG, JA, EF; writing - original draft: CSG , JAG, JRC, JCMG, JA, EF; writing - review & editing: CSG, JAG, JRC, CdW, CMF, GW, JCMG, JA, EF; project administration: JA, EF; funding acquisition: JA, EF.

Conflicts of interest

There are no conflicts to declare.

Acknowledgements

References

1 *WHO Global Tuberculosis Report*, 2023, https://www.who.int/tb/publications/global_report/en/.

2 G. B. Migliori, S. Tiberi, A. Zumla, E. Petersen, J. M. Chakaya, C. Wejse, M. Munoz Torrico, R. Duarte, J. W. Alffenaar, H. S. Schaaf, B. J. Marais, D. M. Cirillo, R. Alagna, A. Rendon, E. Pontali, A. Piubello, J. Figueroa, G. Ferlazzo, A. Garcia-Basteiro, R. Centis, D. Visca, L. D'Ambrosio, G. Sotgiu and N. members of the Global Tuberculosis, MDR/XDR-TB management of patients and contacts: Challenges facing the new decade. The 2020 clinical update by the Global Tuberculosis Network, *Int. J. Infect. Dis.*, 2020, **92**, S15–S25.

3 M. Pai, P. K. Dewan and S. Swaminathan, Transforming tuberculosis diagnosis, *Nat. Microbiol.*, 2023, **8**, 756–759.

4 M. Pai and C. Raison, Transforming the diagnosis of tuberculosis: an editorial board member's opinion at the 15th year of Expert Review of Molecular Diagnostics, *Expert Rev. Mol. Diagn.*, 2015, **15**, 295–298.

5 *WHO Standard: Universal Access to rapid tuberculosis diagnostics*, https://www.who.int/publications/i/item/9789240071315.

6 The unsustainable anachronism of tuberculosis diagnosis, *Lancet Microbe*, 2023, **4**, e379.

7 K. A. Abrahams and G. S. Besra, Mycobacterial cell wall biosynthesis: a multifaceted antibiotic target, *Parasitology*, 2018, **145**, 116–133.

8 P. J. Brennan, Structure, function, and biogenesis of the cell wall of *Mycobacterium tuberculosis*, *Tuberculosis*, 2003, **83**, 91–97.

9 M. Jackson, The mycobacterial cell envelope-lipids, *Cold Spring Harbor Perspect. Med.*, 2014, **4**, a021105.

10 H. L. Hodges, R. A. Brown, J. A. Crooks, D. B. Weibel and L. L. Kiessling, Imaging mycobacterial growth and division with a fluorogenic probe, *Proc. Natl. Acad. Sci. U. S. A.*, 2018, **115**, 5271–5276.

11 B. M. Swarts, C. M. Holsclaw, J. C. Jewett, M. Alber, D. M. Fox, M. S. Siegrist, J. A. Leary, R. Kalscheuer and C. R. Bertozzi, Probing the mycobacterial trehalome with bioorthogonal chemistry, *J. Am. Chem. Soc.*, 2012, **134**, 16123–16126.

12 K. M. Backus, H. I. Boshoff, C. S. Barry, O. Boutureira, M. K. Patel, F. D'Hooge, S. S. Lee, L. E. Via, K. Tahlan, C. E. Barry III and B. G. Davis, Uptake of unnatural trehalose analogs as a reporter for *Mycobacterium tuberculosis*, *Nat. Chem. Biol.*, 2011, **7**, 228–235.

13 A. A. Pohane, C. R. Carr, J. Garhyan, B. M. Swarts and M. S. Siegrist, Trehalose Recycling Promotes Energy-Efficient Biosynthesis of the Mycobacterial Cell Envelope, *mBio*, 2021, **12**(1), DOI: 10.1128/mbio.02801-20.

14 A. Garcia-Heredia, A. A. Pohane, E. S. Melzer, C. R. Carr, T. J. Fiolek, S. R. Rundell, H. C. Lim, J. C. Wagner, Y. S. Morita, B. M. Swarts and M. S. Siegrist, Peptidoglycan precursor synthesis along the sidewall of pole-growing mycobacteria, *eLife*, 2018, **7**, e37243.

15 M. Kamariza, P. Shieh, C. S. Ealand, J. S. Peters, B. Chu, F. P. Rodriguez-Rivera, M. R. Babu Sait, W. V. Treuren, N. Martinson, R. Kalscheuer, B. D. Kana and C. R. Bertozzi, Rapid detection of *Mycobacterium tuberculosis* in sputum with a solvatochromic trehalose probe, *Sci. Transl. Med.*, 2018, **10**, eaam6310.

16 H. L. Parker, R. M. F. Tomas, C. M. Furze, C. S. Guy and E. Fullam, Asymmetric trehalose analogues to probe disaccharide processing pathways in mycobacteria, *Org. Biomol. Chem.*, 2020, **18**, 3607–3612.

17 S. R. Rundell, Z. L. Wagar, L. M. Meints, C. D. Olson, M. K. O'Neill, B. F. Piligian, A. W. Poston, R. J. Hood, P. J. Woodruff and B. M. Swarts, Deoxyfluoro-d-trehalose (FDTre) analogues as potential PET probes for imaging mycobacterial infection, *Org. Biomol. Chem.*, 2016, **14**, 8598–8609.

18 J. T. Belisle, V. D. Vissa, T. Sievert, K. Takayama, P. J. Brennan and G. S. Besra, Role of the major antigen of *Mycobacterium tuberculosis* in cell wall biogenesis, *Science*, 1997, **276**, 1420–1422.

19 R. Kalscheuer, B. Weinrick, U. Veeraraghavan, G. S. Besra and W. R. Jacobs Jr, Trehalose-recycling ABC transporter LpqY-SugA-SugB-SugC is essential for virulence of *Mycobacterium tuberculosis*, *Proc. Natl. Acad. Sci. U. S. A.*, 2010, **107**, 21761–21766.

20 C. Varela, D. Rittmann, A. Singh, K. Krumbach, K. Bhatt, L. Eggeling, G. S. Besra and A. Bhatt, MmpL genes are associated with mycolic acid metabolism in mycobacteria and corynebacteria, *Chem. Biol.*, 2012, **19**, 498–506.

21 Z. Xu, V. A. Meshcheryakov, G. Poce and S. S. Chng, MmpL3 is the flippase for mycolic acids in mycobacteria, *Proc. Natl. Acad. Sci. U. S. A.*, 2017, **114**, 7993–7998.

22 C. M. Furze, I. Delso, E. Casal, C. S. Guy, C. Seddon, C. M. Brown, H. L. Parker, A. Radhakrishnan, R. Pacheco-Gomez, P. J. Stansfeld, J. Angulo, A. D. Cameron and E. Fullam, Structural basis of trehalose recognition by the mycobacterial LpqY-SugABC transporter, *J. Biol. Chem.*, 2021, **296**, 100307.

23 H. N. Foley, J. A. Stewart, H. W. Kavunja, S. R. Rundell and B. M. Swarts, Bioorthogonal Chemical Reporters for Selective *In Situ* Probing of Mycomembrane Components in Mycobacteria, *Angew Chem. Int. Ed. Engl.*, 2016, **55**, 2053–2057.

24 A. A. Pohane, D. J. Moore, I. Lepori, R. A. Gordon, T. O. Nathan, D. M. Gepford, H. W. Kavunja, B. M. Swarts and M. S. Siegrist, A Bifunctional Chemical Reporter for *In Situ* Analysis of Cell Envelope Glycan Recycling in Mycobacteria, *ACS Infect. Dis.*, 2022, **8**, 2223–2231.

25 S. Pena-Zalbidea, A. Y. Huang, H. W. Kavunja, B. Salinas, M. Desco, C. Drake, P. J. Woodruff, J. J. Vaquero and B. M. Swarts, Chemoenzymatic radiosynthesis of 2-deoxy-2-[(18)F]fluoro-d-trehalose ([[(18)F]-2-FDTre): A PET radioprobe for *in vivo* tracing of trehalose metabolism, *Carbohydr. Res.*, 2019, **472**, 16–22.

26 M. Niederweis, Nutrient acquisition by mycobacteria, *Microbiology*, 2008, **154**, 679–692.

27 M. Braibant, P. Gilot and J. Content, The ATP binding cassette (ABC) transport systems of *Mycobacterium tuberculosis*, *FEMS Microbiol. Rev.*, 2000, **24**, 449–467.

28 D. J. Beste, K. Noh, S. Niedenfuhr, T. A. Mendum, N. D. Hawkins, J. L. Ward, M. H. Beale, W. Wiechert and J. McFadden, 13C-flux spectral analysis of host-pathogen metabolism reveals a mixed diet for intracellular *Mycobacterium tuberculosis*, *Chem. Biol.*, 2013, **20**, 1012–1021.

29 D. Debois, K. Hamze, V. Guerineau, J. P. Le Caer, I. B. Holland, P. Lopes, J. Ouazzani, S. J. Seror, A. Brunelle and O. Laprevote, *In situ* localisation and quantification of surfactins in a *Bacillus subtilis* swarming community by imaging mass spectrometry, *Proteomics*, 2008, **8**, 3682–3691.

30 P. Agüi-Gonzalez, S. Jähne and N. T. N. Phan, SIMS imaging in neurobiology and cell biology, *J. Anal. At. Spectrom.*, 2019, **34**, 1355–1368.

31 A. Fearns, D. J. Greenwood, A. Rodgers, H. Jiang and M. G. Gutierrez, Correlative light electron ion microscopy reveals *in vivo* localisation of bedaquiline in *Mycobacterium tuberculosis*-infected lungs, *PLoS Biol.*, 2020, **18**, e3000879.

32 G. L. Fisher, A. L. Bruinen, N. Ogrinc Potocnik, J. S. Hammond, S. R. Bryan, P. E. Larson and R. M. Heeren, A New Method and Mass Spectrometer Design for TOF-SIMS Parallel Imaging MS/MS, *Anal. Chem.*, 2016, **88**, 6433–6440.

33 B. L. Urbanek, D. C. Wing, K. S. Haislop, C. J. Hamel, R. Kalscheuer, P. J. Woodruff and B. M. Swarts, Chemoenzymatic synthesis of trehalose analogues: rapid access to chemical probes for investigating mycobacteria, *ChemBioChem*, 2014, **15**, 2066–2070.

34 R. W. Bassily, R. I. el-Sokkary, B. A. Silwanis, A. S. Nematalla and M. A. Nashed, An improved synthesis of 4-azido-4-deoxy- and 4-amino-4-deoxy-alpha,alpha-trehalose and their epimers, *Carbohydr. Res.*, 1993, **239**, 197–207.

35 S. Monaco, L. E. Tailford, N. Juge and J. Angulo, Differential Epitope Mapping by STD NMR Spectroscopy To Reveal the Nature of Protein-Ligand Contacts, *Angew Chem. Int. Ed. Engl.*, 2017, **56**, 15289–15293.

36 J. D. Carroll, I. Pastuszak, V. K. Edavana, Y. T. Pan and A. D. Elbein, A novel trehalase from *Mycobacterium smegmatis* - purification, properties, requirements, *FEBS J.*, 2007, **274**, 1701–1714.